Eur. Phys. J. C 53, 401–412 (2008)
DOI 10.1140/epjc/s10052-007-0464-7

THE EUROPEAN PHYSICAL JOURNAL C

Regular Article – Theoretical Physics

Analyticity constraints on the strangeness changing vector current and applications to $\tau \to K\pi\nu_\tau$ and $\tau \to K\pi\pi\nu_\tau$

B. Moussallam[a]

Groupe de Physique Théorique, Institut de Physique Nucléaire, CNRS/IN2P3, Université Paris-Sud 11, 91406 Orsay, France

Received: 11 October 2007 / Revised version: 22 October 2007 /
Published online: 29 November 2007 –

Abstract. We discuss matrix elements of the strangeness changing vector current using their relation, due to analyticity, with πK scattering in the P-wave. We take into account experimental phase-shift measurements in the elastic channel as well as results, obtained by the LASS collaboration, on the details of inelastic scattering, which show the dominance of two quasi-two-body channels at medium energies. The associated form factors are shown to be completely determined, up to one flavor symmetry breaking parameter, imposing boundary conditions at $t = 0$ from chiral and flavor symmetries and at $t \to \infty$ from QCD. We apply the results to the $\tau \to K\pi\nu_\tau$ and $\tau \to K\pi\pi\nu_\tau$ amplitudes and compare the former to recent high statistics results from B factories.

PACS. 11.55.Fv; 11.30.Rd; 11.30.Hv; 13.35.Dx

1 Introduction

Decays of the τ to hadrons with strangeness $S = -1$ can be used to determine basic parameters of the standard model such as V_{us} and the mass of the strange quark (see, e.g., [1, 2] for recent updates). The considerable improvement in statistics brought in by Babar and Belle should translate in the near future into much more precise measurements of matrix elements of currents with $S = -1$ than possible at present. In this paper, we re-consider in some detail the relations between the $K\pi$ matrix element of the strangeness changing vector current and $K\pi$ scattering in the P-wave. We shall follow a method applied some time ago by Donoghue, Gasser and Leutwyler (DGL [3]) to the $\pi\pi$ matrix element of the $S = 0$ scalar current (which is not directly accessible to experiment, since the Higgs boson is not very light). For this method to operate, it is necessary that inelastic scattering can be approximated in terms of a finite number of two-body or quasi-two-body channels in a sufficiently large energy range $E \lesssim E_0$. Then, imposing a limited number of constraints at $E = 0$ from chiral symmetry and at $E \gg E_0$ from asymptotic QCD, one can determine the form factor from the T-matrix. In practice, this is done by solving a set of coupled Muskhelishvili–Omnès (MO) integral equations, which are consequences of analyticity properties of the form factors and of time-reversal invariance.

Recently, this method was implemented in the case of the $K\pi$ scalar form factor [4]: in this case, inelasticity in the S-wave is saturated by the $K\eta$ and $K\eta'$ channels. One motivation for our interest in the vector form factor is the availability of good experimental data from the LASS collaboration on both elastic [5] and inelastic $K\pi$ scattering [6–8] in the P-wave. In particular, these works show that in an energy range $E \lesssim 2.5\,\mathrm{GeV}$, inelasticity is dominated by two quasi-two-body channels: $K^*\pi$ and $K\rho$. This makes it possible to probe the DGL method by comparing its results with experimental data from τ decays. The spectral function for $\tau \to K\pi\nu_\tau$ can be described, of course, by a simple Breit–Wigner ansatz in the vicinity of the $K^*(892)$ resonance, where scattering is nearly perfectly elastic. Away from the resonance, however, this is no longer true. In the energy region $E \ll M_{K^*}$ the spectral function gets dominated by the scalar component [9] (as it is less suppressed by phase-space than the vector component). In the energy region $E \gg M_{K^*}$ it is important to correctly treat inelastic effects. Another motivation for this work is in view of applications to the three-body non-leptonic B decays $B \to K\pi\pi$. In kinematical configurations where the kaon and one pion are quasi-aligned, factorization can presumably be justified [10], and the amplitude gets expressed in terms of $K\pi$ vector and scalar form factors [11].[1]

The plan of the paper is as follows. After introducing some notation for the form factors involved we discuss the construction of the T-matrix from fits to the experimental πK scattering data. Three-channel unitarity is enforced using the K-matrix method, and proper fla-

[a] e-mail: moussall@ipno.in2p3.fr

[1] In the context of B decays, the usefulness of appealing to descriptions more sophisticated than Breit–Wigner combinations for scalar form factors was pointed out in [12].

vor symmetry and low energy behavior are enforced starting from a resonance chiral Lagrangian. Next, we introduce the MO integral equations satisfied by the form factors and discuss their resolution. This necessitates making a plausible ansatz for the T-matrix at high energies. The ansatz determines the number of conditions to be imposed in order to determine the form factors from solving the integral equations. We shall use three conditions at $E = 0$ and one asymptotic condition. Finally, the results are displayed and compared with recent experimental measurements.

2 Strangeness changing vector current form factors

The object that will mainly interest us is the $K\pi$ matrix element of the strangeness changing vector current

$$\begin{aligned}&\left\langle K^+(p_K)|\bar{u}\gamma^\mu s|\pi^0(p_\pi)\right\rangle \\ &\quad = f_+^{K^+\pi^0}(t)\,(p_K+p_\pi)^\mu + f_-^{K^+\pi^0}(t)\,(p_K-p_\pi)^\mu\,,\end{aligned} \tag{1}$$

with $t = (p_K - p_\pi)^2$ and we shall denote the vector form factor as

$$H_1(t) \equiv f_+(t) = \sqrt{2} f_+^{K^+\pi^0}(t)\,. \tag{2}$$

As we shall discuss below $K\pi$ inelastic scattering in the P-wave is dominated by two quasi-two-body channels: $K^*\pi$ and ρK. This leads us to introduce the associated vector current matrix elements

$$\begin{aligned}\left\langle K^{*+}(p_V,\lambda)|\bar{u}\gamma_\mu s|\pi^0(p_\pi)\right\rangle &= \epsilon_{\mu\nu\alpha\beta} e^{*\nu}(\lambda) p_V^\alpha p_\pi^\beta H_2(t)\,,\\ \left\langle \rho^0(p_V,\lambda)|\bar{u}\gamma_\mu s|K^-(p_K)\right\rangle &= -\epsilon_{\mu\nu\alpha\beta} e^{*\nu}(\lambda) p_V^\alpha p_K^\beta H_3(t)\end{aligned} \tag{3}$$

(we have chosen different signs in the definition of H_2 and H_3 such that only plus signs appear in subsequent equations). In the following, isospin symmetry breaking will be neglected. From the isospin decomposition of $K^+\pi^0$ it follows that

$$\left\langle K^+\pi^0|\bar{u}\gamma_\mu s|0\right\rangle = \sqrt{\frac{1}{3}}\left\langle [K\pi]_{\frac{1}{2}}|\bar{u}\gamma_\mu s|0\right\rangle\,, \tag{4}$$

and analogous relations hold for $K^*\pi$, $K\rho$. In order to derive the unitarity equations satisfied by the form factors H_1, H_2 and H_3 it is convenient to focus on one of the spatial components of the vector current, say $\mu = 3$, and go to center-of-mass (CMS) frame of the meson pair. In this frame, the current matrix elements introduced above can be expressed as follows:

$$\left\langle [K\pi]_{\frac{1}{2}}|\bar{u}\gamma^3 s|0\right\rangle = \sqrt{6}\cos\theta_0 q_{K\pi}(t) H_1(t)\,, \tag{5}$$

where $q_{K\pi}$ is the modulus of the CMS momentum of the meson pair and θ_0 is the polar angle of the momentum vector with respect to a fixed frame. Similarly, the matrix elements that involve one vector meson read

$$\begin{aligned}\left\langle [K^*(\lambda)\pi]_{\frac{1}{2}}|\bar{u}\gamma^3 s|0\right\rangle &= \mathrm{i}\eta^*\sqrt{\frac{3}{2}}\,\sin\theta_0\sqrt{t}\,q_{K^*\pi}(t)\,H_2(t)\,,\\ \left\langle [\rho(\lambda)K]_{\frac{1}{2}}|\bar{u}\gamma^3 s|0\right\rangle &= \mathrm{i}\eta^*\sqrt{\frac{3}{2}}\,\sin\theta_0\sqrt{t}\,q_{\rho K}(t)\,H_3(t).\end{aligned} \tag{6}$$

Here, η is an arbitrary phase that can be introduced in the definition of the vector meson polarization vector

$$\mathbf{e}^*(\lambda=\pm1) = \frac{\eta^*}{\sqrt{2}}\begin{pmatrix}-\lambda\cos\theta_0\cos\phi_0 - \mathrm{i}\sin\phi_0\\ -\lambda\cos\theta_0\sin\phi_0 + \mathrm{i}\cos\phi_0\\ \lambda\sin\theta_0\end{pmatrix}\,, \tag{7}$$

(θ_0, ϕ_0 being the polar angles of the vector meson momentum). In the following, we shall set $i\eta^* = 1$. We have also taken the following convention for the Levi-Civita tensor:

$$\epsilon_{0123} = 1\,. \tag{8}$$

The explicit dependence on θ_0 displayed above in (5) and (6) indicates that these matrix elements concern the angular momentum state $J = 1$ of the meson pair.

3 $K\pi$ scattering in P-wave with n-channel unitarity

3.1 Experimental situation

Detailed partial-wave analysis of $K\pi \to K\pi$ scattering (in the energy range $E \lesssim 2.5$ GeV) have been performed based on high statistics production experiments $Kp \to K\pi N$ in [5, 13]. The LASS collaboration has also performed production experiments $K^-p \to K\,2\pi N$ and $K^-p \to K\,3\pi N$ [6–8], which provide information on inelastic $K\pi$ scattering. These, however, are not as precise as for elastic scattering and mainly concern resonance properties in the various partial waves. In the S-wave, $K\pi$ scattering is elastic to a good approximation up to the $K\eta'$ threshold [5, 13], indicating that $K\eta'$ is the main inelastic channel. Inelasticity in the P-wave starts at somewhat smaller energy than in the S-wave and the results of [6, 7] suggest that $K^*\pi$ is the main inelastic channel, as it is enhanced by two resonances $K^*(1410)$ and $K^*(1680)$ (following the nomenclature of the PDG [14]). The latter resonance was observed to couple essentially to three channels: $K\pi$, $K^*\pi$ as well as $K\rho$ [14]. This indicates that $K\rho$ should be also taken into account as a significant inelastic channel in the P-wave although its coupling to $K^*(1410)$ was found to be small. The experimental results on the branching ratios of the $K^*(1410)$ and $K^*(1680)$ are collected in Table 1.

The $K\pi \to K\eta$ amplitude was studied in [8] and found to be very small in the P-wave and not to display any resonant effect. The coupling of $K\eta'$ to resonances with $J^{PC} = 1^{--}$ is proportional to the sine of the mixing angle

Table 1. Experimental decay branching ratios (in percent units) for the resonances $K^*(1410)$ and $K^*(1680)$ quoted in the PDG

	$K\pi$	$K^*\pi$	$K\rho$
$K^*(1410)$	6.6 ± 1	> 40	< 7
$K^*(1680)$	38.7 ± 2.5	$29.9^{+2.2}_{-4.7}$	$31.4^{+4.7}_{-2.1}$

and thus should also be suppressed. These results suggest that a plausible description of $K\pi$ scattering in the P-wave with n-channel unitarity can be performed (up to energies $E \lesssim 2.5$ GeV) by retaining as inelastic channels the two quasi-two-body channels with one vector meson: $K^*\pi$ and $K\rho$.

3.2 Lagrangian for vector resonances and pseudo-scalar mesons

It is useful to express the resonance contribution to scattering in terms of coupling constants that are known in other contexts and it is also useful to impose chiral constraints at low energy. For this reason, let us start from the following Lagrangian, which was used in the context of the chiral expansion [15–17]. It includes the nonet of the light vector mesons encoded in a matrix V_μ and the light pseudo-scalars encoded in a chiral matrix u_μ and involves two coupling constants g_V and σ_V:

$$\mathcal{L}^{(1)} = \mathcal{L}_K^{(1)} + \mathcal{L}_V^{(1)} + \mathcal{L}_\sigma^{(1)}\,, \tag{9}$$

with

$$\begin{aligned}
\mathcal{L}_K^{(1)} &= \frac{-1}{4}\mathrm{tr}\left(V_{\mu\nu}V^{\mu\nu} - 2M_V^2 V_\mu V^\mu\right),\\
\mathcal{L}_V^{(1)} &= \frac{-\mathrm{i}}{2} g_V\,\mathrm{tr}\left(V_{\mu\nu}[u_\mu, u_\nu]\right),\\
\mathcal{L}_\sigma^{(1)} &= \frac{1}{2}\sigma_V\,\epsilon^{\mu\nu\rho\sigma}\mathrm{tr}\left(V_\mu\{u_\nu, V_{\rho\sigma}\}\right),
\end{aligned} \tag{10}$$

and $V_{\mu\nu} = \nabla_\mu V_\nu - \nabla_\nu V_\mu$. In [16,17], for example, the following values are quoted for the coupling constants (based on the extended NJL model):

$$g_V \simeq 0.083\,, \quad \sigma_V \simeq 0.25\,, \tag{11}$$

which should serve as a guide as to the orders of magnitudes. Let us denote an excited vector resonance by $V_\mu^{(n)}$, we can write down the following coupling terms:

$$\begin{aligned}
\mathcal{L}_V^{(n)} &= \frac{-\mathrm{i}}{2} g_V(n)\,\mathrm{tr}\left(V_{\mu\nu}^{(n)}[u_\mu, u_\nu]\right),\\
\mathcal{L}_\sigma^{(n)} &= \frac{1}{2}\sigma_V(n)\,\epsilon^{\mu\nu\rho\sigma}\mathrm{tr}\left(V_\mu^{(n)}\{u_\nu, V_{\rho\sigma}\}\right).
\end{aligned} \tag{12}$$

These terms do not involve the quark mass matrix and, therefore, have exact SU(3) flavor symmetry. Experimental results on K^* resonances indicate that flavor symmetry can sometimes be substantially broken, as in the case of the $K^*(1410)$ (see Table 1). We do not try to write down all possible Lagrangian terms that break flavor symmetry, but eventually we shall implement such effects at the level of the fits. We also do not consider explicitly the possibility of many more terms that involve further derivatives acting on the vector or on the chiral fields. Again, such terms, which give rise to polynomial energy dependence, may be implemented phenomenologically as "background" contributions in the fits.

3.3 Resonance contributions to $K\pi$ scattering

Let us recall the constraints introduced by the conservation of parity. The $K\pi$ system, at first, in the P-wave has parity -1. The action of the parity operator on a state formed from a vector meson and a pseudo-scalar meson involves the helicity [18,19],

$$\mathcal{P}|V(\lambda)P\rangle_J = (-)^{J-1}|V(-\lambda)P\rangle_J\,. \tag{13}$$

For $J = 1$, the following combination is the only one that has negative parity:

$$\psi_- = \frac{1}{\sqrt{2}}\left(|V(1)P\rangle_{J=1} - |V(-1)P\rangle_{J=1}\right). \tag{14}$$

We shall need the partial-wave expansion of the scattering amplitudes in a situation where the initial state CMS momentum has polar angles θ_0, ϕ_0 and the final state has polar angles θ, ϕ [18,19]

$$\begin{aligned}
\langle V(\lambda)P|T|K\pi\rangle &= 16\pi\sum_{J,M}(2J+1)\left(q_{VP}\,q_{K\pi}\right)^J\\
&\quad\times\left\langle V(\lambda)P|T^J|K\pi\right\rangle \mathcal{D}^{*J}_{M,\lambda}(\phi,\theta)\mathcal{D}^J_{M,0}(\phi_0,\theta_0)\,,\\
\langle V(\lambda)P|T|V'(\lambda')P\rangle &= 16\pi\sum_{J,M}(2J+1)\left(q_{VP}\,q_{V'P}\right)^J\\
&\quad\times\left\langle V(\lambda)P|T^J|V'(\lambda')P\right\rangle \mathcal{D}^{*J}_{M,\lambda}(\phi,\theta)\mathcal{D}^J_{M,\lambda'}(\phi_0,\theta_0)\,.
\end{aligned} \tag{15}$$

We have factored out explicitly the angular momentum barrier factors in the definition of the partial-wave T-matrix elements: this is necessary for non-diagonal matrix elements in order to ensure good analytical behavior for the partial-wave T-matrix [20]. For simplicity, we also define the diagonal elements in the same manner e.g.

$$\begin{aligned}
\langle K\pi|T|K\pi\rangle = 16\pi\sum_{J,M}(2J+1)\left(q_{K\pi}\right)^{2J}&\left\langle K\pi|T^J|K\pi\right\rangle\\
&\times\mathcal{D}^{*J}_{M,0}(\phi,\theta)\mathcal{D}^J_{M,0}(\phi_0,\theta_0)\,.
\end{aligned} \tag{16}$$

Let us number the three relevant channels in our construction as

$$1 \longrightarrow K\pi\,, \quad 2 \longrightarrow K^*\pi\,, \quad 3 \longrightarrow K\rho\,, \tag{17}$$

Using the Lagrangian introduced above (10) and (12) it is not difficult to compute the resonance contributions to

the various T-matrix elements. The resulting amplitude can be written in a compact form that displays the usual resonance structure,

$$T^1_{ij,\mathrm{r}} = \sum_n \frac{g_\mathrm{r}(n,i)g_\mathrm{r}(n,j)}{M_n^2 - s}\,, \tag{18}$$

with

$$\begin{aligned} g_\mathrm{r}(n,1) &= \frac{g_V(n)}{\sqrt{16\pi}}\left(\frac{\sqrt{s}}{F_\pi}\right)^2 \\ g_\mathrm{r}(n,2) &= \frac{\sigma_V(n)}{\sqrt{16\pi}}\frac{\sqrt{2s}}{F_\pi}(1+\delta_{n1}) \\ g_\mathrm{r}(n,3) &= \frac{-\sigma_V(n)}{\sqrt{16\pi}}\frac{\sqrt{2s}}{F_\pi}\,. \end{aligned} \tag{19}$$

The relations between channel 2 and channel 3 matrix elements are consequences of exact flavor symmetry as implemented in the Lagrangians (10) and (12). The energy dependence of these effective coupling constants is reliable only for small values of s ($s \ll M^2_{K^*}$) where chiral symmetry constraints (as encoded in the construction of the Lagrangian) are relevant. In practice, we shall implement a simple cutoff function by replacing

$$\sqrt{s} \longrightarrow \frac{\sqrt{s}\left(1 + b_n \frac{\sqrt{s}}{M_n}\right)}{1 + b_n \frac{s}{M_n^2}} \tag{20}$$

in (19). This cutoff function has the correct behavior at small s and effectively replaces $\sqrt{s}$ by the resonance mass M_n otherwise.

3.4 K-matrix fits to the experimental data

We may implement n-channel unitarity in a simple way, using the K-matrix method (e.g. [21]). Starting from a real, symmetric K-matrix we define the $J = 1$ T-matrix in the following way (suppressing the J superscript):

$$T = (1 - \mathrm{i}K\Sigma Q^2)^{-1}K\,, \tag{21}$$

where Q^2 and Σ are diagonal matrices

$$(Q^2)_{ij} = \delta_{ij}q_i^2, \quad \Sigma_{ij} = \delta_{ij}\frac{2q_i}{\sqrt{s}}\,, \tag{22}$$

q_i being the CMS momentum in channel i. Indeed, it not difficult to verify that the S-matrix , which is defined as follows:

$$S = 1 + 2\mathrm{i}\sqrt{\Sigma}\,Q\,T\,Q\,\sqrt{\Sigma} \tag{23}$$

is unitary

$$SS^\dagger = 1 \tag{24}$$

and encodes the proper $J = 1$ angular momentum barrier factors.

3.4.1 A first simple fit

The most detailed experimental results concern the $K\pi$ elastic channel. We used the results of [5] on the amplitudes $K^-\pi^+ \to K^-\pi^+$ in the energy range $E \leq 2.5$ GeV and those of [13] on the isospin 3/2 amplitude. Let us first perform a simple fit including just three resonances in the K-matrix, i.e., we set $K_{ij} = T^1_{ij,\mathrm{r}}$ using the formulas (18) and (19). We find a qualitatively acceptable result (see Fig. 1) with the following resonance parameters:

M_n	$g_V(n)$	$\sigma_V(n)$
0.894	0.0714	0.0989
1.719	0.0103	−0.1857
2.247	0.0126	−0.3069

(25)

(masses are in GeV and the coupling constants are dimensionless). In this fit we have taken $b_n = \infty$ (see (20)) i.e. $\sqrt{s}$ is replaced by M_n. This fit does find a resonance corresponding to $K^*(1680)$ in addition to the $K^*(892)$ but prefers to locate the third resonance at a higher energy

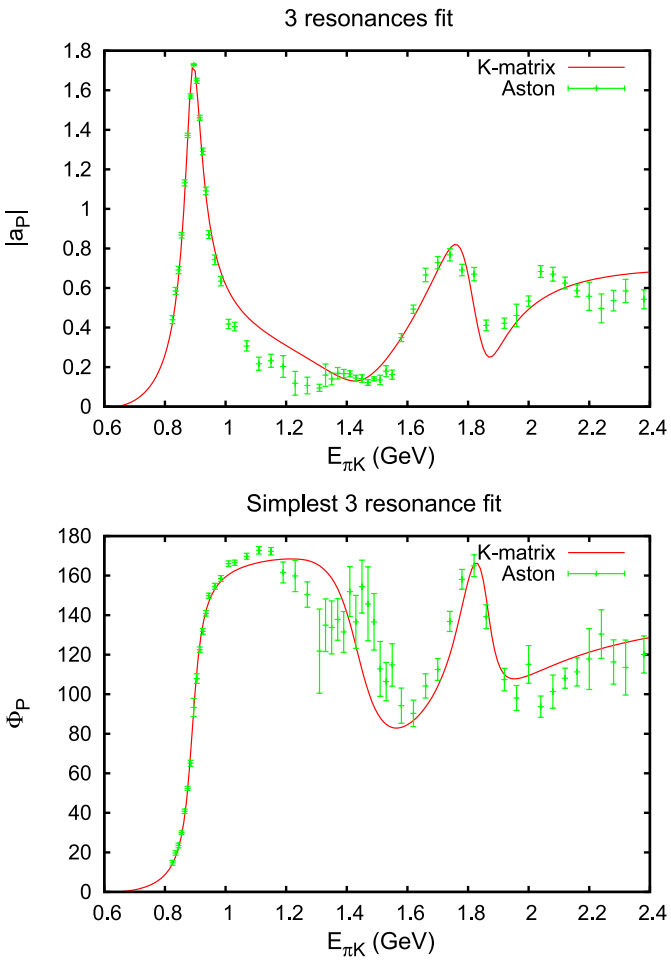

Fig. 1. K-matrix fit to the $K\pi \to K\pi$ data of [5] with three resonances. a_P is the modulus of the $K^-\pi^+ \to K^-\pi^+$ amplitude and Φ_P is the phase

rather than at 1.4 GeV. Obviously, though, the energy region between 1 and 1.5 GeV is where the data are not very well described (the overall $\chi^2/\mathrm{dof} = 7.4$).

3.4.2 More sophisticated fits

Including just one more resonance does not improve the situation very much. In order to obtain significantly better fits we shall include a fourth resonance in addition to non-resonant background terms. There are many physical sources for such terms. We have seen, for instance, that the coupling constants may carry energy dependence. In addition, we expect contributions associated with the left-hand cut, i.e. arising from meson exchanges in the crossed channels. We parametrize such contributions in the following, simplistic, way:

$$K_{11}^{\mathrm{back}} = \frac{a_1 s}{1+s^3}$$
$$K_{12}^{\mathrm{back}} = \frac{s(a_2+a_3 s)}{1+s^3}$$
$$K_{13}^{\mathrm{back}} = \frac{a_4 s}{1+s^3}\,. \qquad (26)$$

For the other K-matrix elements we do not introduce any background dependence. We have tried many possibilities but, clearly, the amount of experimental data is insufficient for probing in detail all the matrix elements of the K-matrix, so one must make admittedly arbitrary simplifying assumptions. We found that setting non-zero background terms for K_{11} K_{12} and K_{13} is the most economic way (in terms of number of parameters) to achieve a good fit. In addition to the elastic $K\pi$ data, we try to reproduce the constraints on the inelastic channels in the resonance regions (see Table 1). These data imply strong flavor symmetry violation in the region of the $K^*(1410)$ resonance. We account for this fact by relaxing the symmetry relation $g_{\mathrm{r}}(n,3) = -g_{\mathrm{r}}(n,2)$ (see (19)) for $n = 2$. Instead of this relation, we suppress the coupling to channel 3 (i.e. $K\rho$) by simply setting

$$g_{\mathrm{r}}(n,3) = 0\,, \qquad (27)$$

when $n = 2$.

Altogether, this fit contains 16 parameters and allows for a rather satisfactory fit to the Aston et al. data, which has a $\chi^2/\mathrm{dof} \simeq 1.8$. We note that the fourth resonance present in this fit effectively acts essentially as an additional source of background at lower energies: it should not necessarily be interpreted as a true physical resonance (in fact no corresponding resonance is listed in the PDG). The numerical results for the best fit parameters are collected in Table 2. One observes that the values of $g_V(1)$ and $\sigma_V(1)$ are in reasonable agreement with the ENJL predictions from [16,17]. Figure 2 shows the comparison of the fit results with the experimental data. The improvement with respect to the result of the simpler fit shown in Fig. 1 is obvious, particularly in the energy region [1,1.4] GeV. Moreover this fit is able to reproduce, qualitatively at least, the experimental results concerning the inelastic channels recalled in Table 1. This is illustrated in Fig. 3,

Table 2. Results for the fit parameters concerning the four resonances and the background as described in Sect. 3.4.2

n	M_n	$g_V(n)$	$\sigma_V(n)$	a_n
1	0.8962	0.72820×10^{-1}	0.26080	3.3906
2	1.3789	0.52523×10^{-2}	–0.56075	18.373
3	1.7300	0.69365×10^{-2}	–0.21774	–9.2048
4	2.2739	0.12044×10^{-2}	–0.29360	2.8318

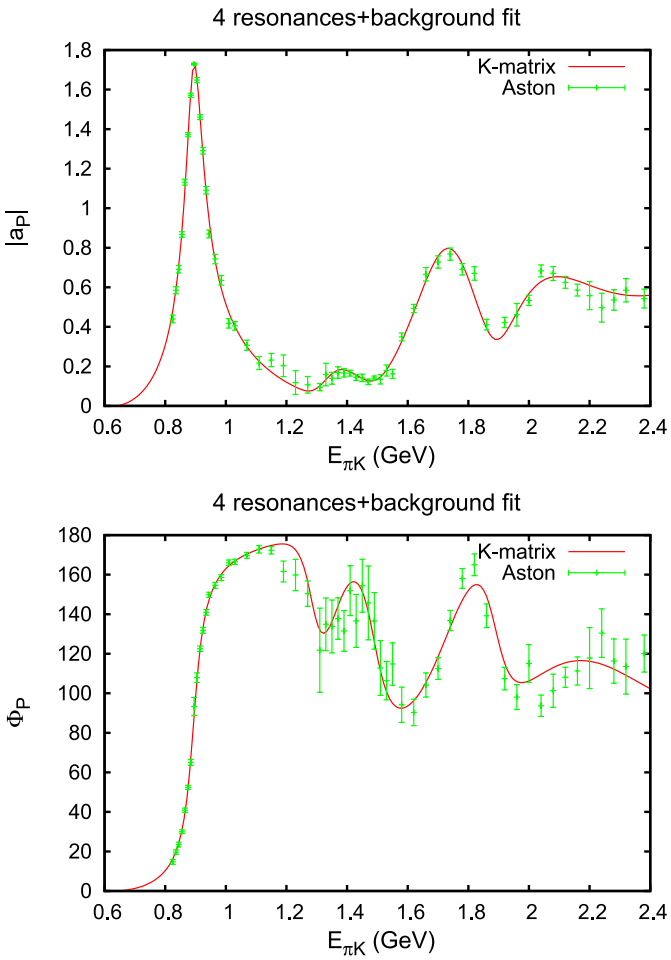

Fig. 2. K-matrix fit to the $K\pi \to K\pi$ data of [5] with four resonances plus background, as described in Sect. 3.4.2

which shows the moduli of the transition S-matrix elements and, for the elastic channel $1 - S_{11}$ (the cross-sections are proportional to the squares of these quantities). Indeed, the figure shows that in the energy region corresponding to the $K^*(1410)$ the matrix element S_{12} shows a clear resonance peak while S_{13} shows no peak. In the energy region of the $K^*(1680)$ resonance these two matrix elements display peaks of the same height (this was imposed as a constraint in the fit) and the peak in the elastic channel is slightly higher.

In the very small s region, finally, our T-matrix is expected to be qualitatively reasonable but certainly not very accurate because of the lack of constraints from experimen-

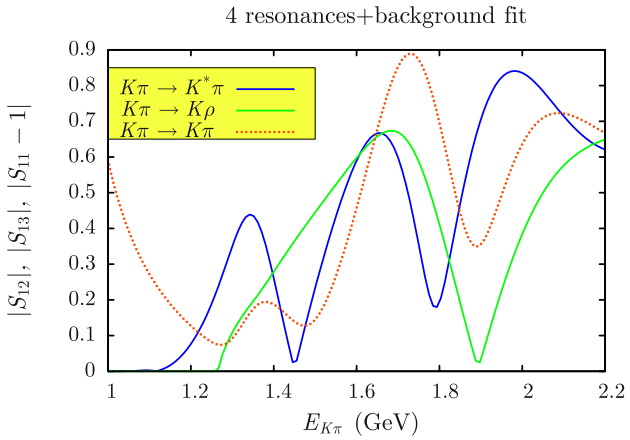

Fig. 3. Results from the fit described in Sect. 3.4.2 concerning the inelastic S-matrix element moduli $|S_{12}|$ and $|S_{13}|$ as well as the elastic matrix element modulus $|1-S_{11}|$

tal data in the threshold region. The πK scattering length, for instance, is found to be

$$a_1^{1/2} = 0.025\,, \tag{28}$$

which has the correct order of magnitude but is slightly larger than the result from ChPT (at order p^6) [22]: $a_1^{1/2} = 0.018$.

4 The $K\pi$ vector form factor from n-channel MO equations

4.1 Unitarity equations

The Muskhelishvili–Omnès equations derive from the fact that, firstly, each of the form factors $H_1(t)$, $H_2(t)$ and $H_3(t)$ satisfy an unsubtracted dispersion relation because they are analytic functions in the variable t except for a right-hand cut[2] [23] and they decrease for $t \to \infty$ faster than $1/t$. Secondly, one can express the imaginary parts of the form factors in terms of T-matrix elements using time-reversal invariance. Let us briefly repeat the derivation in the case of a scalar operator $\mathcal{O}$ that is $\mathcal{T}$-invariant

$$\mathcal{T}\mathcal{O}\mathcal{T}^{-1} = \mathcal{O}\,. \tag{29}$$

We consider the imaginary part of the matrix element between the vacuum and a state $|m\rangle$, which we take to be an "out" state

$$2\mathrm{i}\mathrm{Im}\,{}_{\rm out}\langle m|\mathcal{O}|0\rangle = {}_{\rm out}\langle m|\mathcal{O}|0\rangle - {}_{\rm out}\langle m|\mathcal{O}|0\rangle^*\,, \tag{30}$$

Using the fact that $\mathcal{T}$ is antiunitary and transforms an "out" sate into an "in" state, it is not difficult to transform the second term on the right-hand side in (30) and recover the usual unitarity expression for the imaginary part

$$\mathrm{Im}\,{}_{\rm out}\langle m|\mathcal{O}|0\rangle = \frac{1}{2}\sum_n T^*_{mn\,\rm out}\langle n|\mathcal{O}|0\rangle\,. \tag{31}$$

In reality, we shall use operators that carry space-time indices and thus are not $\mathcal{T}$-invariant. It is however easy to see that the $\mathcal{T}$-variation of the operator is compensated by the $\mathcal{T}$-variation of the momenta p_i in the state $|m>$ such that (31) remains valid for the form factors. For a given energy of the state $|m\rangle_{\rm out}$ a finite number of states $|n\rangle_{\rm out}$ contribute to the sum in the right-hand side (Watson's theorem [24] follows if the energy is lower than the first inelastic threshold). If we truncate the summation in (31) and insert the imaginary parts into the dispersion relations we obtain a closed set of MO integral equations for the form factors.

4.2 Application to $K\pi$, $K^*\pi$, ρK vector form factors

We start from the general expression (31), apply it to the operator $\bar{u}\gamma^3 s$ and retain three states in the sum: $K\pi$, $K^*\pi$ and ρK. We then use the formulas (5) and (6) and the partial-wave expansions (15) of the T-matrix elements and compute the phase-space integrals. As expected, only the $J=1$ partial wave contributes, and after a small calculation the unitarity equations for $H_1(t)$, $H_2(t)$ and $H_3(t)$ are obtained. They can be written as follows, in matrix form:

$$\mathrm{Im}\begin{pmatrix} H_1 \\ H_2 \\ H_3 \end{pmatrix} = \tau^{-1}T^*Q^2\Sigma\tau\begin{pmatrix} H_1 \\ H_2 \\ H_3 \end{pmatrix}\,, \tag{32}$$

where T is the 3×3 $J=1$ T-matrix, the diagonal matrices Q^2 and Σ are defined in (22) and τ is also a diagonal matrix:

$$\tau = \mathrm{diag}\,(1, \sqrt{t}, \sqrt{t})\,. \tag{33}$$

The MO integral equation set then is derived by combining (32) with the unsubtracted dispersion relations satisfied by the form factors

$$\begin{pmatrix} H_1(t) \\ H_2(t) \\ H_3(t) \end{pmatrix} = \frac{1}{\pi}\int_{(m_K+m_\pi)^2}^{\infty}\frac{\mathrm{d}t'}{t'-t}\mathrm{Im}\begin{pmatrix} H_1(t') \\ H_2(t') \\ H_3(t') \end{pmatrix}\,. \tag{34}$$

We recall here that the following matrix plays a role when discussing existence and multiplicity of the solutions to the MO equations [25, 26]:

$$\tilde{S} = 1 + 2\mathrm{i}\tau^{-1}TQ^2\Sigma\tau\,. \tag{35}$$

This matrix differs from the S-matrix , as defined in (23), but the determinants of the two matrices are equal

$$\det\tilde{S} = \det S\,. \tag{36}$$

[2] In reality, the form factors H_2 and H_3 could display anomalous thresholds since they involve an unstable particle. We ignore this possibility in our analysis.

4.3 Asymptotic conditions on the T-matrix

The MO equations obeyed by the form factors are coupled, homogeneous singular integral equations with a kernel linear in the T-matrix. The mathematical properties of such equations are exposed in Muskhelishvili's book [25]. In particular, the number of independent solutions N is given by the index of the integral operator, which can be expressed in terms of the sum of the eigenphases $\delta_i(t)$ of the S-matrix. For an $n \times n$ S-matrix,

$$\sum_1^n [\delta_j(\infty) - \delta_j(0)] = N\pi \,. \tag{37}$$

In order to determine the form factors from the integral equations one must therefore impose N independent conditions. In our case one has $n = 3$ and the S-matrix has been constrained from experimental input up to $E_0 \simeq 2.5$ GeV. We make the key assumption here that E_0 is sufficiently large, so that the asymptotic regime for the T-matrix is set up for values of E not much larger than E_0. At $E = E_0$ the sum of the eigenphases is $\sum \delta_i(E_0) \simeq 3.5\pi$. We therefore expect the index N to be either 3 or 4. We choose to adopt an asymptotic condition that has an index $N = 4$. This will enable us to impose four conditions on the form factor. Three of these use the values at the origin of the form factors, $H_i(0)$. We shall discuss below how these values are constrained by experiment. As a fourth condition, we can enforce the behavior of $f_+(t)$ at infinity. In QCD, ignoring flavor symmetry breaking, one should have [27, 28]

$$f_+(-Q^2)\big|_{Q^2\to\infty} \sim \frac{16\pi\sqrt{2}\,\alpha_{\rm s}(Q^2)F_\pi^2}{Q^2} \,. \tag{38}$$

We do not attempt to reproduce the logarithmic running of $\alpha_{\rm s}$, and actually use (38) with a constant value $\bar{\alpha}_{\rm s} = 0.2$. The condition (38) is then easily implemented in the form of a sum rule:

$$\frac{1}{\pi}\int_{(m_K+m_\pi)^2}^{\infty} {\rm d}t' {\rm Im}\, H_1(t') = 16\pi\sqrt{2}\bar{\alpha}_{\rm s}\, F_\pi^2 \,. \tag{39}$$

In the region $t \geq t_0$ one must use a parametrization that respects the unitarity of the S-matrix . For this purpose, we write the S-matrix in exponential form,

$$S = \exp(2{\rm i}H) \,, \tag{40}$$

where H is a real, symmetric matrix. We then define the interpolation on the matrix H such that

$$\begin{aligned} &\lim_{t\to\infty} H_{12}(t), H_{13}(t), H_{23}(t) = 0 \,, \\ &\lim_{t\to\infty} H_{11}(t) + H_{22}(t) + H_{33}(t) = 4\pi \,, \end{aligned} \tag{41}$$

using the simple interpolating function

$$\begin{aligned} H_{ij}(t) = &\left(\frac{t_0}{t}\right)^\gamma \left(\alpha_{ij} + \beta_{ij}\left(\frac{t_0}{t}\right)^\gamma\right) \\ &+ H_{ij}(\infty)\left(1 - \left(\frac{t_0}{t}\right)^\gamma\right)^2 \,. \end{aligned} \tag{42}$$

The parameters α_{ij} and β_{ij} are determined so as to ensure continuity of $H_{ij}(t)$ and its first derivative at $t = t_0$. Consistent with the assumption made above on the setting of the asymptotic regime, the parameter γ must be larger than one: in practice, we shall take $\gamma = 2$. The condition on the trace of H still leaves some freedom as to the behavior of each diagonal element. We shall consider a plausible scenario in which the asymptotic eigenphases satisfy

$$\delta_1(\infty) = 2\pi \,, \quad \delta_2(\infty) = \delta_3(\infty) = \pi \,, \tag{43}$$

where δ_1 is the largest eigenphase at $t = t_0$. The three eigenphases are shown in Fig. 4.

4.4 Conditions at $t = 0$

In this section we discuss the experimental constraints on the form factor components at $t = 0$. The component $H_1(0) = f_+(0)$, firstly, is well known from ChPT to very close to 1, the result at $O(p^4)$ was computed in [29],

$$f_+(0) = 0.977 \quad ({\rm ChPT}O(p^4)) \,. \tag{44}$$

We note that ChPT computations at order p^6 have been performed [30], but the p^6 coupling constants involved are not yet well known. The remaining two form factor components involve vector mesons. We shall argue that their values at $t = 0$ can still be evaluated reasonably well by appealing, in addition to chiral expansion arguments, to a leading large N_c approximation. In the chiral limit, flavor symmetry is exact, and the following relation holds between a charged current matrix element and an electromagnetic current one:

$$\left\langle K^{*+}|\bar{u}\,\gamma^\mu\, s|\pi^0\right\rangle = \frac{3\sqrt{2}}{2}\left\langle \rho^+|j^\mu_{\rm EM}|\pi^+\right\rangle \,. \tag{45}$$

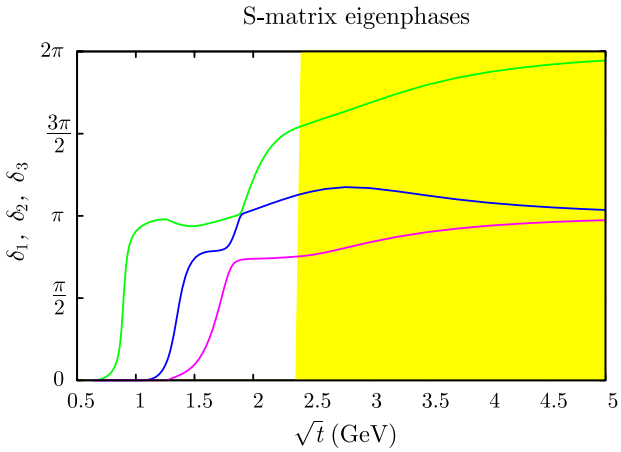

Fig. 4. Eigenphases of the S-matrix: the *left part* of the figure shows the region determined from experiment, the *right part* (colored in *yellow*) shows the asymptotic interpolation region. The asymptotic condition here is $\sum \delta_i(\infty) = 4\pi$

This relation implies that one can relate $H_2(0)$ and $H_3(0)$ to the radiative width of the charged ρ meson,

$$|H_2(0)| = |H_3(0)| = \left(\frac{27}{2}\frac{\Gamma_{\rho^+\to\gamma\pi^+}}{\alpha\, p_{\gamma\pi}^3}\right)^{\frac{1}{2}} . \qquad (46)$$

Using the experimental value [14] of the radiative decay width

$$\Gamma_{\rho^+\to\gamma\pi^+} = 68 \pm 7\,\mathrm{keV} \qquad (47)$$

gives

$$|H_2(0)| = |H_3(0)| = 1.54 \pm 0.08\,\mathrm{GeV}^{-1} . \qquad (48)$$

This method does not fix the sign of $H_2(0)$. For this purpose, we can appeal to a simple vector-dominance picture applied, e.g., to the vertex function $\langle\gamma|\bar{u}\gamma_\mu d|\pi^-\rangle$. In such a picture $H_2(0)$ gets related to the ABJ anomaly [31, 32],

$$H_2(0) = -H_3(0) = \frac{N_c}{8\pi^2}\,\frac{1}{\sqrt{2}f_V F_\pi} \simeq 1.50\,\mathrm{GeV}^{-1} . \qquad (49)$$

We observe that the absolute value of $H_2(0)$ in the VMD model is in rather good agreement with the one deduced from experiment.

We can try to refine these estimates by taking into account the breaking of flavor symmetry to first order in the quark masses. For this purpose, let us write down an effective Lagrangian,

$$\begin{aligned}\mathcal{L} = \epsilon_{\mu\nu\alpha\beta}\Big\{ & h_V\,\mathrm{tr}\,\left(V^\mu\{u^\nu, f_+^{\alpha\beta}\}\right) \\ & + \frac{a}{M_V^2}\,\mathrm{tr}\,\left([V^\mu,u^\nu]\left[\chi^+, f_+^{\alpha\beta}\right]\right) \\ & + \frac{b}{M_V^2}\,\mathrm{tr}\,\left(\{V^\mu,u^\nu\}\left\{\chi^+, f_+^{\alpha\beta}\right\}\right) \\ & + \frac{c}{M_V^2}\,\mathrm{tr}\,([V^\mu,\chi^+][u^\nu,f_+^{\alpha\beta}])\Big\} . \end{aligned} \qquad (50)$$

We have used the same notation as in [16, 17] for the first term in this Lagrangian. Flavor symmetry breaking effects can be encoded into three independent Lagrangian terms: this holds in the leading large N_c approximation (since multiple trace terms are suppressed). We can then constrain the coupling constants h_V, a, b and c by considering the radiative decays $\rho^+\to\pi^+\gamma$, $K^{*+}\to K^+\gamma$, and $K^{*0}\to K^0\gamma$. The corresponding amplitudes, computed from the Lagrangian (50), have the expressions

$$A(\rho^+\to\pi^+\gamma) = \frac{4\sqrt{2}}{3F_\pi}h_V^{\mathrm{eff}}, h_V^{\mathrm{eff}} = h_V + \frac{4m_\pi^2}{M_V^2}b \qquad (51)$$

and

$$\begin{aligned} A(K^{*+}\to K^+\gamma) &= \frac{4\sqrt{2}}{3F_K}h_V^{\mathrm{eff}} - \frac{16\sqrt{2}}{3F_\pi}\frac{m_K^2-m_\pi^2}{M_V^2}(2b-3c)\,, \\ A(K^{*0}\to K^0\gamma) &= \frac{-8\sqrt{2}}{3F_K}h_V^{\mathrm{eff}} - \frac{32\sqrt{2}}{3F_\pi}\frac{m_K^2-m_\pi^2}{M_V^2}b\,. \end{aligned} \qquad (52)$$

The following experimental results are available [14] for the K^* mesons radiative decays:

$$\begin{aligned}\Gamma(K^{*+}\to K^+\gamma) &= 116 \pm 12\,\mathrm{keV}\,, \\ \Gamma(K^{*0}\to K^0\gamma) &= 50 \pm 5\,\mathrm{keV}\,, \end{aligned} \qquad (53)$$

which, together with the result (47) allows one to determine three coupling constants,

$$\begin{aligned} h_V^{\mathrm{eff}} &= 0.0356 \pm 0.0018, \\ b &= 0.0010 \pm 0.0015, \\ c &= 0.0032 \pm 0.0013\,. \end{aligned} \qquad (54)$$

Let us now compute our form factor components from the Lagrangian (50), obtaining

$$\begin{aligned} H_2(0) &= \frac{4}{F_\pi}h_V^{\mathrm{eff}} - \frac{16}{F_\pi}\frac{m_K^2-m_\pi^2}{M_V^2}(a-b+c)\,, \\ H_3(0) &= -\frac{4}{F_K}h_V^{\mathrm{eff}} - \frac{16}{F_\pi}\frac{m_K^2-m_\pi^2}{M_V^2}(a+b)\,. \end{aligned} \qquad (55)$$

These expressions show that $H_2(0)$ and $H_3(0)$ depend on the symmetry breaking parameter a, which is left undetermined by the analysis of radiative vector meson decays. Numerically, using the values (54) we find

$$\begin{aligned} H_2(0) &= 1.41 \pm 0.09 - 65.4\,a\,\mathrm{GeV}^{-1}\,, \\ H_3(0) &= -1.34 \pm 0.07 - 65.4\,a\,\mathrm{GeV}^{-1}\,. \end{aligned} \qquad (56)$$

We expect the parameter a to have the same order of magnitude as the other two symmetry breaking parameters, i.e. $|a| < 10^{-2}$.

5 Solutions and comparisons with experimental results

5.1 Solving the MO equations

The integral equations (32) and (34) can be solved numerically by discretizing the integrals. This must be done in a way that guarantees a precise evaluation of the principal-value integrals. For this purpose, we use expansions over Legendre polynomials and exact expressions for the principal-value integrals of these. More details can be found in [26]. One then arrives at a set of $M\times M$ homogeneous linear ordinary equations. The Muskhelishvili conditions on the number of solutions imply that the determinant of the system must vanish (if it does not, then the only solution would be the trivial identically vanishing one) and the associated matrix must have N (with $N=4$ in our case) zero eigenvalues. In practice, because of discretization and round-off errors no eigenvalue vanishes exactly, but one does have N eigenvalues that are very small in magnitude. A numerically stable way to proceed is to enlarge the system to an $(M+N)\times M$ one by adding N constraints on the form factors as equations and then solve the new system using the singular value decomposition method. We obtained precise results with $M \gtrsim 100$

and we used values of M up to 400. Several correctness and accuracy tests can be performed. In particular, while exact solutions are not known for general T-matrices, the value of the determinant of the matrix formed from N independent solutions can be expressed in analytical form [25, 26] in terms of S-matrix elements.

5.2 Results for τ decays

The vector form factor $f_+(t)$ can be probed using the τ decay mode $\tau \to K\pi\nu_\tau$. The energy distribution of the $K\pi$ pair has the following expression, which involves $f_+(t)$ as well as the scalar form factor $f_0(t)$:

$$\frac{\mathrm{d}\Gamma_{K\pi}(t)}{\mathrm{d}\sqrt{t}} = \frac{V_{us}^2 G_\mathrm{F}^2 m_\tau^3}{128\pi^3} q_{K\pi}(t) \left(1-\frac{t}{m_\tau^2}\right)^2 \times \left[\left(1+\frac{2t}{m_\tau^2}\right)\frac{4q_{K\pi}^2(t)}{t}|f_+(t)|^2 + \frac{3(m_K^2-m_\pi^2)^2}{t^2}|f_0(t)|^2\right], \quad (57)$$

where the definition of f_0, in terms of the form factors introduced in (1) is

$$f_0(t) = \sqrt{2}\left[f_+^{K^+\pi^0}(t) + \frac{t}{m_K^2-m_\pi^2} f_-^{K^+\pi^0}(t)\right]. \quad (58)$$

The contribution of f_0 is kinematically suppressed except for very small values of t. Let us begin by fixing the symmetry breaking parameter a from the integrated width. Assuming exact isospin symmetry one has

$$\Gamma_{K\pi} = 3\Gamma_{K^-\pi^0} = \frac{3}{2}\Gamma_{\overline{K}_0\pi^-}. \quad (59)$$

The following value for the rate is quoted by the PDG [14]:

$$R_{K\pi}^{\mathrm{PDG}} = (13.5 \pm 0.05)\,10^{-3}. \quad (60)$$

The most recent results from the Babar and Belle collaborations [33, 34] tend, however, to point towards a slightly smaller value

$$R_{K\pi}^{\mathrm{Babar}} = (12.48 \pm 0.009 \pm 0.054)\,10^{-3}, \quad R_{K\pi}^{\mathrm{Belle}} = (12.12 \pm 0.006 \pm 0.039)\,10^{-3} \quad (61)$$

(assuming isospin symmetry). These results can be reproduced with our vector form factor[3] by having the parameter a in the range

$$a = \left(-7.0^{+0.7}_{-2.0}\right) \times 10^{-3}. \quad (62)$$

The central value corresponds to the PDG result and the value $a = -9.0 \times 10^{-3}$ reproduces Belle's central figure for the rate. The energy distribution in the decay $\tau \to K\pi\nu_\tau$ has been measured for the first time by the Aleph collaboration [36, 37]. The Belle collaboration has recently measured the distribution in energy for the decay $\tau^- \to K_S^0\pi^-\nu_\tau$ with considerably higher statistics [34] (approximately a thousand times larger). The Babar collaboration has also presented results for the energy distribution for $\tau^- \to K^-\pi^0\nu_\tau$ [33] but the data corrected for background are not publicly available. Data from Babar on $\tau^- \to K_S^0\pi^-\nu_\tau$ have been analyzed in a thesis [38] but the results have not yet been published.

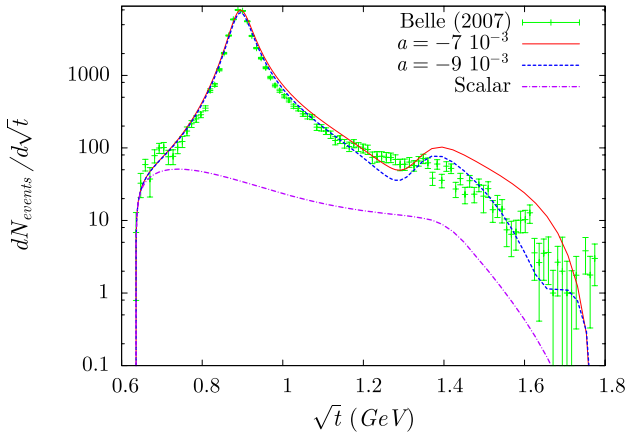

Fig. 5. Results for the energy dependence of the τ decay rate $\tau \to K\pi\nu_\tau$ using the vector form factor as discussed in the text for two values of the symmetry breaking parameter a compared with the result from Belle [34]. The contribution from the scalar form factor f_0 is shown as a *dash-dot curve*

The result from our construction is compared with the result of Belle[4] in Fig. 5 for two values of a. In addition to the (dominant) contribution from the vector form factor, we have also included the contribution from the scalar form factor, which we computed following [4]. The parameter a affects the size of the $K^*(892)$ peak (which controls essentially the value of the integrated decay rate) and also the shape of the form factor in the inelastic region. We find that it is possible to reproduce both the integrated decay rate and the shape of the energy distribution above the K^* mass reasonably well. The solutions in the region $\sqrt{t} \gtrsim 1.4$ GeV are sensitive to the assumptions made on the S-matrix in the asymptotic domain. For instance, if we choose an asymptotic condition with $N = 3$ rather than $N = 4$ we cannot get agreement with experiment when $\sqrt{t} \gtrsim 1.4$ GeV by varying a.

It is instructive to compare also our result for the vector form factor with that obtained by Belle from a fit to their data. This comparison avoids the problem of the acceptance (which is taken into account in their fit) but one must keep in mind that there is some model dependence in this determination (a model independent separation of the vector and scalar form factors requires to analyze angular distributions). In [34] five different fits, using descriptions of the form factors f_+ and f_0 à la Kühn and Santamaria [39], have been performed. In Fig. 6 we compare our result for the modulus of the vector form factor with the experimen-

[3] In applications to τ decays we use for V_{us} the value such that $V_{us}f_+(0) = 0.2167$ quoted by the averaging group [35].

[4] The data shown have been corrected for background but not for acceptance, which we have assumed to be approximately energy independent.

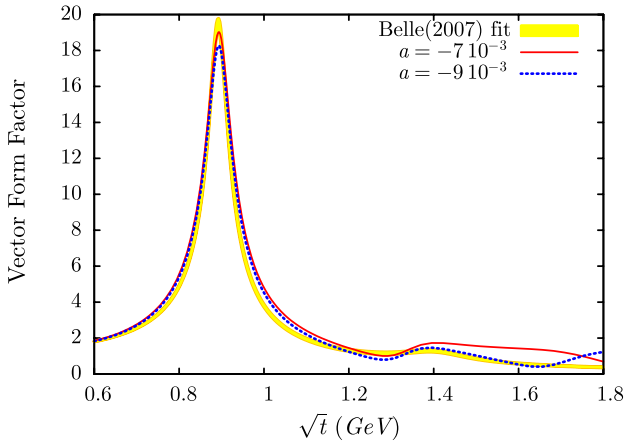

Fig. 6. The *yellow band* represents the modulus of the vector form factor determined from a four parameter fit in [34]. It is compared with our determination for two values of the symmetry breaking parameter a

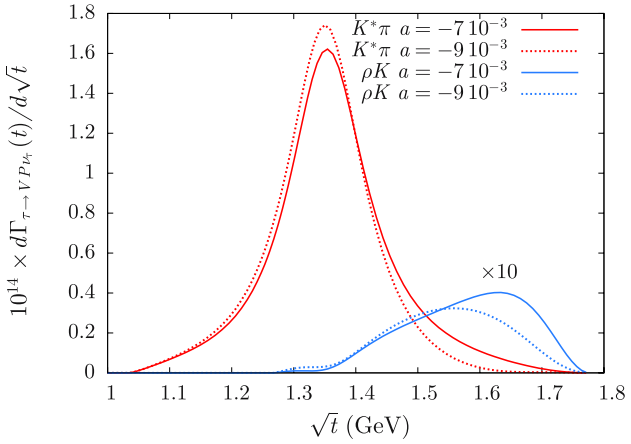

Fig. 7. Results for the energy distribution of the τ decay width into $K^*\pi$ and $K\rho$ (rescaled by a factor of 10) via vector current from our model, for two values f the symmetry breaking parameter a

tal determination based on the fit that includes two vector resonances: $K^*(892)$ and $K^*(1410)$ for the vector form factor and one scalar resonance: $K_0^*(800)$ for the scalar form factor. For clarity, we have presented our model's result as one curve corresponding to the best fit to the LASS data but, obviously, one should keep in mind the uncertainties of these data, which are sometimes sizable, e.g., in the 1.3 GeV region (see Fig. 2).

This comparison deserves a comment. In the $K^*(892)$ region one expects to observe some isospin symmetry breaking effects since the $K\pi$ system in $\tau \to K\pi\nu_\tau$ is in a charged state while the experimental data from LASS concern $K\pi$ in a neutral state. Figure 6 shows a visible difference concerning the width, which is narrower for the K^{*+} than for the K^{*0}. Somewhat surprisingly, no difference is seen concerning the mass. In fact, the mass resulting from Belle's fit: $M_{K^{*+}} = 895.47 \pm 0.20 \pm 0.44 \pm 0.59$ differs by about 4 MeV from the mass quoted in the PDG: $M_{K^{*+}} = 891.66 \pm 0.26$, which is based on hadronic production experiments. This shift in the K^{*+} mass was reported earlier by CLEO [40] but remains to be confirmed. It could be a similar effect to the one observed for the ρ meson mass.

The model also generates predictions for τ decays into $K^*\pi$ and $K\rho$ via vector current. The energy distribution of the decay width for $K^*\pi$ reads, in terms of the form factor H_2,

$$\frac{\mathrm{d}\Gamma_{K^*\pi}}{\mathrm{d}\sqrt{s}} = \frac{V_{us}^2 G_\mathrm{F}^2 m_\tau^3}{32\pi^3}(q_{K^*\pi})^3 \left(1 - \frac{t}{m_\tau^2}\right)^2 \left(1 + \frac{2t}{m_\tau^2}\right) |H_2(t)|^2 , \tag{63}$$

and an exactly similar expression holds for $K\rho$ in terms of H_3. The results from our construction are plotted in Fig. 7. The figure shows that the $K^*(1410)$ appears very clearly in the $K^*\pi$ channel. The τ decay into $K\rho$ (via vector current) is comparatively strongly suppressed. These features reflect the constraints that we have used in the construction of the T-matrix based on the LASS experiments. The results for the integrated rates are

$$R\,(\tau \to K^*\pi\nu_\tau)_V = (1.37 \pm 0.02)\,10^{-3}, \quad R\,(\tau \to K\rho\nu_\tau)_V = (4.5 \pm 3.0)\,10^{-5}, \tag{64}$$

where the errors are estimated by simply varying the parameter a. Our result for $R(\tau \to K^*\pi\nu_\tau)_V$ is seen to agree with the one quoted by the Aleph collaboration [36, 37],

$$R^{\mathrm{Aleph}}\,(\tau \to K^*(1410)\nu_\tau \to K\pi\pi\nu_\tau) = \left(1.4^{+1.3+0.0}_{-0.9-0.4}\right) 10^{-3}, \tag{65}$$

which, however, is not very precise.

5.3 Some results at $t = 0$

For values of t near $t = 0$, experimental results on $f_+(t)$ can be obtained from K_{l3} decays and several new experiments have been performed recently. One usually defines the slope and curvature parameters from the Taylor expansion:

$$f_+(t) = f_+(0)\left(1 + \lambda' \frac{t}{m_{\pi^+}^2} + \frac{1}{2}\lambda'' \frac{t^2}{m_{\pi^+}^4} + \ldots\right). \tag{66}$$

The results that we get for λ' and λ'' are

$$\lambda' = \left(26.05^{+0.21}_{-0.58}\right)\,10^{-3}, \quad \lambda'' = \left(1.29^{+0.01}_{-0.04}\right)\,10^{-3}, \tag{67}$$

where the errors, again, simply reflect the range of variation of the parameter a (the lower values correspond to $a = -9 \times 10^{-3}$). They compare reasonably well with the average (performed in [35]) over the recent experiments

$$\lambda'_{\mathrm{exp}} = (24.8 \pm 1.1)\,10^{-3}, \quad \lambda''_{\mathrm{exp}} = (1.61 \pm 0.45)\,10^{-3}. \tag{68}$$

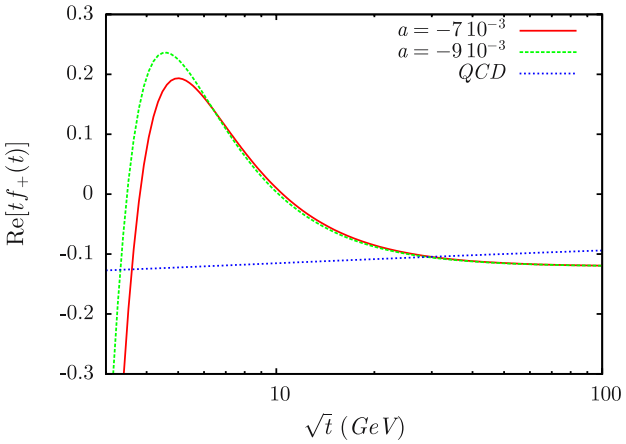

Fig. 8. Real part of the product $tf_+(t)$ resulting from our solution of the MO equations compared with asymptotic QCD prediction

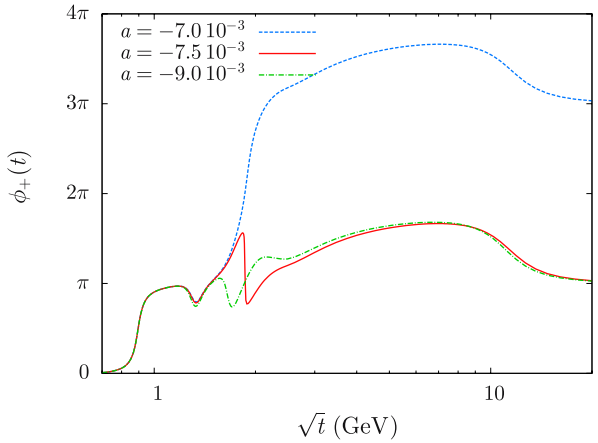

Fig. 9. Illustration of the changing behaviour of the phase of $f_+(t)$ at large t when the parameter a varies

The results (67) can also be compared with the predictions recently presented in [9],[5]

$$\lambda' = 26.2 \times 10^{-3}\,, \quad \lambda'' = 1.37 \times 10^{-3} \quad ([9])\,. \qquad (69)$$

5.4 Some remarks on the asymptotic region

When $t \to \infty$, the MO equations driven by the T-matrix behaving as discussed in Sect. 4.3 can be shown to imply that $tf_+(t)$ goes to a constant. We have constrained this constant, via (39), in order to correctly reproduce QCD in an average sense. Figure 8 displays the real part of the product $tf_+(t)$ obtained from the numerical solution of the equations. The figure also shows the asymptotic QCD expectation (analytically continued to the timelike region). One sees that $tf_+(t)$ indeed goes to a constant, but the asymptotic behavior sets in at fairly large values of t. A similar feature was observed in the case of the pion vector form factor, which was discussed in [41].

Another remark concerns the phase of $f_+(t)$ (let us denote it as $\phi_+(t)$). It is often assumed that $\phi_+(t)$ should go to π as t goes to infinity (e.g. [42, 43]), while compatibility with asymptotic QCD simply implies that it should go to π modulo 2π. Let us recall that if the phase of $f_+(t)$ goes to π at infinity, f_+ can be expressed in terms of its phase as a minimal Omnès representation. In our construction, we find that the behavior of the phase at infinity depends on the value of a. This is illustrated in Fig. 9. For the central value of a the phase actually goes to 3π at infinity. When a gets slightly smaller, a transition occurs and the phase goes to π. Again here, the asymptotic behavior is reached for rather large values of t.

6 Conclusions

In this work, we have considered matrix elements between light states of the strangeness changing vector current. Such quantities are now becoming accessible to experiment, with rather good precision in a rather large energy range from hadronic τ decays. There are possible applications to certain three-body B decays as well. From a theoretical point of view, one can establish relations between two-body form factors and the scattering matrix not only at very low energy in the elastic scattering region (Watson's theorem) but also at somewhat higher energies provided that inelastic scattering is dominated by two-body channels. This was shown to be the case for πK scattering in the P-wave by the LASS collaboration [5–7] in the energy range $E \lesssim 2.5$ GeV. Similar properties hold for $\pi\pi$ scattering in the S-wave and also for πK scattering in the S-wave and were used to construct scalar form factors [3, 4]. Those results, however, have not been compared with experimental data.

We have constructed a three-channel T-matrix, which satisfies unitarity, from fits to the large amount of data on $\pi K \to \pi K$ scattering in the P-wave and satisfying the experimental constraints on inelastic scattering. In the region $E \geq 2.5$ GeV, one must make a plausible guess. We impose a smooth interpolation such that the MO operator has index $N = 4$. The three form factors can then be determined by solving the system of MO equations and applying four constraints. We have used the three values at the origin, which we have argued to be determined, making use of chiral and flavor symmetries, up to one symmetry breaking parameter a. As a fourth constraint, we used asymptotic QCD behavior for the form factor f_+.

The result of this construction for the form factor $f_+(t)$ compares reasonably well with the recent determination by the Belle collaboration. The agreement in the inelastic region is not quite trivial to achieve. Indeed, the $K^*(1680)$ resonance appears as a very large effect in $\pi K \to \pi K$ scattering while it is suppressed in the form factor. Varying the parameter a outside of the range allowed from the in-

[5] We converted the numerical values taking into account that the expansion formula (66) is used in [9] with $m_\pi = 138$ MeV rather than $m_\pi = 139.57$ MeV.

tegrated $\tau \to K\pi\nu_\tau$ rate also destroys the agreement in the energy distribution. The result in the domain $\sqrt{t} \geq 1.4\,\mathrm{GeV}$ is also sensitive to how the T-matrix behaves above 2.5 GeV. In the region of the $K^*(892)$ resonance, there are some discrepancies. While these could be due to isospin breaking effects, they seem to concern the width rather than the mass of the $K^*(892)$, which is unexpected. Finally, we made predictions for the total rates and the energy distributions for the vector current contribution to the τ decays $\tau \to K^*\pi\nu_\tau$ and $\tau \to \rho K \nu_\tau$.

Acknowledgements. The author would like to thank D. Epifanov for making the numerical values of the Belle measurements available and for correspondence. This work is supported by the European commission MRTN FLAVIAnet [MRTN-CT-2006035482].

References

1. E. Gamiz, M. Jamin, A. Pich, J. Prades, F. Schwab, Nucl. Phys. Proc. Suppl. **169**, 85 (2007) [hep-ph/0612154]
2. K. Maltman, C.E. Wolfe, Phys. Lett. B **650**, 27 (2007) [hep-ph/0701037]
3. J.F. Donoghue, J. Gasser, H. Leutwyler, Nucl. Phys. B **343**, 341 (1990)
4. M. Jamin, J.A. Oller, A. Pich, Nucl. Phys. B **622**, 279 (2002) [hep-ph/0110193]
5. D. Aston et al., Nucl. Phys. B **296**, 493 (1988)
6. D. Aston et al., Nucl. Phys. B **247**, 261 (1984)
7. D. Aston et al., Nucl. Phys. B **292**, 693 (1987)
8. D. Aston et al., Phys. Lett. B **201**, 169 (1988)
9. M. Jamin, A. Pich, J. Portoles, Phys. Lett. B **640**, 176 (2006) [hep-ph/0605096]
10. Talks given by M. Beneke, I. Stewart at the "Three-body Charmless B decays Workshop", February 1–3 (2006), LPNHE, Paris, http://lpnhe-babar.in2p3.fr/3BodyCharmlessWS/
11. B. El-Bennich, A. Furman, R. Kamiński, B. Loiseau, L. Leśniak, B. Moussallam, work in progress
12. S. Gardner, U.G. Meißner, Phys. Rev. D **65**, 094004 (2002) [hep-ph/0112281]
13. P. Estabrooks, R.K. Carnegie, A.D. Martin, W.M. Dunwoodie, T.A. Lasinski, D.W.G. Leith, Nucl. Phys. B **133**, 490 (1978)
14. Particle Data Group, W.M. Yao et al., J. Phys. G **33**, 1 (2006)
15. G. Ecker, J. Gasser, H. Leutwyler, A. Pich, E. de Rafael, Phys. Lett. B **223**, 425 (1989)
16. J. Prades, Z. Phys. C **63**, 491 (1994)
17. J. Prades, Z. Phys. C **11**, 571 (1999) [Erratum] [hep-ph/9302246]
18. M. Jacob, G.C. Wick, Ann. Phys. **7**, 404 (1959)
19. M. Jacob, G.C. Wick, Ann. Phys. **281**, 774 (2000)
20. W.R. Frazer, J.R. Fulco, Phys. Rev. **117**, 1603 (1960)
21. R.H. Dalitz, S.F. Tuan, Ann. Phys. **10**, 307 (1960)
22. J. Bijnens, P. Dhonte, P. Talavera, JHEP **0405**, 036 (2004) [hep-ph/0404150]
23. G. Barton, Introduction to Dispersion Techniques in Field Theory (Bejamin, New York, 1965)
24. K.M. Watson, Phys. Rev. **88**, 1163 (1952)
25. N.I. Muskhelishvili, Singular Integral Equations (P. Noordhof, Groningen, The Netherlands, 1953)
26. B. Moussallam, Eur. Phys. J. C **14**, 111 (2000) [hep-ph/9909292]
27. S.J. Brodsky, G.P. Lepage, Phys. Rev. D **22**, 2157 (1980)
28. A. Duncan, A. Mueller, Phys. Rev. D **21**, 1636 (1980)
29. J. Gasser, H. Leutwyler, Nucl. Phys. B **250**, 517 (1985)
30. J. Bijnens, P. Talavera, Nucl. Phys. B **669**, 341 (2003) [hep-ph/0303103]
31. S. Adler, Phys. Rev. **177**, 2426 (1969)
32. J.S. Bell, R. Jackiw, Nuovo Cim. A **60**, 47 (1969)
33. BABAR Collaboration, B. Aubert et al., arXiv:0707.2922 [hep-ex]
34. Belle Collaboration, D. Epifanov et al., arXiv:0706.2231 [hep-ex]
35. FlaviaNet Working Group on Kaon Decays, M. Moulson, talk given at the 4th International Workshop on the CKM Unitarity Triangle (CKM 2006), Nagoya, Japan, 12–16 Dec 2006, hep-ex/0703013
36. ALEPH Collaboration, R. Barate et al., Eur. Phys. J. C **10**, 1 (1999) [hep-ex/9903014]
37. ALEPH Collaboration, R. Barate et al., Eur. Phys. J. C **11**, 599 (1999) [hep-ex/9903015]
38. A.J. Lyon, Studies of the strange hadronic tau decay tau- - - > K0(S) pi-nu/tau using the BaBar detector, PhD thesis, University of Manchester (2004)
39. J.H. Kühn, A. Santamaria, Z. Phys. C **48**, 445 (1990)
40. CLEO Collaboration, G. Bonvicini et al., Phys. Rev. Lett. **88**, 111803 (2002) [hep-ex/0111095]
41. J.F. Donoghue, E.S. Na, Phys. Rev. D **56**, 7073 (1997) [hep-ph/9611418]
42. F.J. Yndurain, Phys. Lett. B **578**, 99 (2004)
43. F.J. Yndurain, Phys. Lett. B **586**, 439 (2004) [Erratum] [hep-ph/0309039]